PCCP

Structural Evolution of Water-in-Propylene Carbonate Mixtures Revealed by Experimental Raman Spectroscopy and Molecular Dynamics

Journal:	*Physical Chemistry Chemical Physics*
Manuscript ID	CP-ART-05-2023-002181.R1
Article Type:	Paper
Date Submitted by the Author:	11-Jul-2023
Complete List of Authors:	Clark, Jessica; The Ohio State University, Department of Chemistry & Biochemistry Bowling-Charles, Tai; The Ohio State University, Department of Chemistry & Biochemistry Proma, Shamma Jabeen; The Ohio State University, Department of Chemistry & Biochemistry Biswas, Biswajit; The Ohio State University, Department of Chemistry & Biochemistry Limmer, David; University of California Berkeley, Chemistry; UC Berkeley Allen, Heather; The Ohio State University, Department of Chemistry and Biochemistry

Structural Evolution of Water-in-Propylene Carbonate Mixtures Revealed by Experimental Raman Spectroscopy and Molecular Dynamics

Jessica B. Clark†, Tai Bowling-Charles†, Shamma Jabeen Proma†, Biswajit Biswas†, David T. Limmer‡, Heather C. Allen†*

†Department of Chemistry & Biochemistry, The Ohio State University, Columbus, Ohio 43210, USA

‡Department of Chemistry, University of California, Berkeley, California 94720, USA

Materials Sciences Division, Lawrence Berkeley National Laboratory, Berkeley, California 94720, USA

Chemical Sciences Division, Lawrence Berkeley National Laboratory, Berkeley, California 94720, USA

Kavli Energy NanoScience Institute, Berkeley, California 94720, USA

Corresponding author

* Heather C. Allen, allen@chemistry.ohio-state.edu

Abstract

The liquid structure of systems wherein water is limited in concentration or through geometry is of great interest in various fields such as biology, materials science, and electrochemistry. Here, we present a combined polarized Raman and molecular dynamics investigation of the structural changes that occur as water is added incrementally to propylene carbonate (PC), a polar, aprotic solvent that is important in lithium-ion batteries. Polarized Raman spectra of PC solutions were collected for water mole fractions $0.003 \leq \chi_{water} \leq 0.296$, which encompasses the solubility range of water in PC. The novel approach taken to the study of water-in-PC mixtures herein provides additional hydrogen bond and solvation characterization of this system that has not been achieveable in previous studies. Analysis of the polarized carbonyl Raman band in conjunction with simulations demonstrated that the bulk structure of the solvent remained unperturbed upon the addition of water. Experimental spectra in the O-H stretching region were decomposed through Gaussian fitting into sub-bands and studies on dilute HOD in H_2O. With the aid of simulations, we identified these different bands as

water arrangements having different degrees of hydrogen bonding. The observed water structure within PC indicates that water tends to self-aggregate, forming a hydrogen bond network that is distinctly different from the bulk and dependent on concentration. For example, at moderate concentrations, the most likely aggregate structures are chains of water molecules, each with two hydrogen bonds on average.

Introduction

The structure and properties of water within complex environments is of fundamental interest due to its potential to reveal new insights into the dynamic hydrogen bonding network of water and its many anomalous bulk properties which have confounded the community for decades.[1,2] When water is limited in quantity and geometric configuration by physical or chemical constraints, its properties often differ significantly from those of a bulk liquid.[3–5] It is necessary to understand how the properties of water are altered in these environments in order to establish the limits at which bulk properties begin to arise or break down. This knowledge aids in the understanding of the fundamental microscopic mechanisms that govern water's macroscopic properties.

There has been significant study of the structure of water in systems with well-defined boundaries such as in confinement within reverse micelles[3,6] carbon nanotubes,[7,8] metal-organic frameworks,[9,10] and silica pores[11]. However, the study of water in disordered, dynamic environments such as binary mixtures has been more limited.[12–17] Notable exceptions are water in ionic liquids, which have gained significant interest in recent years.[16–22] Studies of ionic liquid binary mixtures with water reveal nanoscopic aggregation of water within the solvent (i.e. formation of a nanoconfined "water pocket") that is strongly dependent on the chemical structure of the ionic liquid.[16–18,23] Using small angle x-ray and neutron scattering, Abe and coworkers found that the "water pocket" formed in the ionic liquid [C_4mim][NO_3] has slow orientational dynamics and weak hydrogen bonds due to the nanoconfined nature of the system.[17]

In contrast to studies of water in ionic liquids, studies investigating binary mixtures of dilute water dispersed in dipolar, aprotic, organic solvents are more limited.[12,14,24–29] Studies in the late 1960s showed that within partially chlorinated hydrocarbon solvents, water formed small clusters with itself (dimers to tetramers), but there was disagreement concerning the primary species.[28] In comparison to the previous study, Shultz and coworkers revealed that water exists as monomers in the non-polar solvent CCl_4 and that that the rotational motion of the monomers is greatly restricted by the solvating environment.[30] In hydrogen bond accepting solvents such as amines and ketones, water self-association has been observed and formation of the trimer species has been proposed.[12,27] In such systems, water exists under dynamic confinement by the polar, aprotic solvents due to a balance of intermolecular interactions. The structural characterization of these binary mixtures provides information that is critical in multiple materials applications such as ion solvation in electrolyte solutions.[31–33]

Propylene carbonate (**PC**) is a commonly used solvent in lithium-ion batteries, where it is typically mixed with linear carbonates to provide optimal charge stabilization and transport.[33–41] One of the pitfalls of these electrolyte solutions is the hygroscopicity of PC, which can result in water contamination. This contamination causes hydrolysis of $LiPF_6$ to HF and significantly impedes battery performance.[42,43] Studies have also shown that the addition of PC or water to electrolyte solutions greatly impacts the ion conductivity, which in some cases is dictated by the types of ion pairs formed in solution.[44–48] It is still unclear how the addition of water to PC impacts the PC/Li ion pair formation and thus the conductivity. Therefore, it is critical to understand the solvation structure of water in PC.[36,40–43] PC has unique chemical and physical properties that make it a well-suited solvent for studies of water structure under dynamic confinement. PC has a high dielectric constant (64.40 at 25 °C) and dipole moment (4.94 D).[49] Unlike many other similar organic solvents, it cannot act as a hydrogen

bond donor, only as an acceptor. As a result, some of the chemical complexity that exists in hydrogen bond donating solvents is removed, enabling simpler structural characterization.

The behavior of water in a binary solution with PC has been evaluated in two notable previous studies, yet there is disagreement between the proposed water structure. The first study by Grunwald and coworkers evaluated mixtures of PC and water in the concentration range 0-3.5 m ($\chi_{water} \leq 0.26$) using FTIR and ^{1}H NMR spectroscopies.[12] From this study, it was concluded that water primarily forms monomers and dimers when solvated in PC and that cyclic trimers or other highly coordinated species do not form. Then in a second study, Dei and coworkers used surface tensiometry, differential scanning calorimetry, and FTIR spectroscopy to investigate mixtures of PC and water in the molar ratio range of $0.041 \leq \chi_{water} \leq 0.33$.[14] In contrast to the former study, the authors claim that monomers and dimers are the primary species only under very limited water conditions ($\chi_{water} < 0.14$). Once the water concentration exceeds the threshold, the authors observe that water shifts from being fully solvated by PC to forming stronger solute-solute interactions in trimers structures, a finding that is inconsistent with the older work by Grunwald et al. In the present work, we expand the knowledge of water structure within PC beyond what has been accomplished using FTIR spectroscopy to help address the conflicting conclusions that have been reached in previous works. This is achieved by combining MD simulations with polarized Raman spectroscopy, a technique that provides complementary vibrational information to FTIR spectroscopy.

In the analysis of water's structure, vibrational spectroscopy is often employed due to its high sensitivity to the local environment of the molecule(s) being studied.[50–52] Raman spectra, as opposed to FTIR, provides more highly differentiable O-H spectral features given the same instrument resolving power due to the differing selection rules. It is therefore highly suitable for observing subtle changes in water's hydrogen bond structure.[50,53] An additional advantage that Raman spectroscopy provides is the ability to observe polarized responses that result from local vibrational symmetry.[54]

The analysis of such responses from PC enables the determination of its liquid structure, which was unclear in prior work that relied on FTIR peak shifts alone.[12,14]

In its bulk liquid state, water forms four hydrogen bonds in an approximately tetrahedral geometry, on average. These hydrogen bonds are highly dynamic and fluctuate on a picosecond timescale causing a distribution of configurations with varying bond strengths.[55,56] As a result, the O-H stretching vibrational bands are broad and complex to interpret due to their close overlap with one another. It is generally accepted that this convolution of bands is a result of several component bands that correspond to different hydrogen-bonded water assemblies.[14,20,51,52,55–61] Therefore, this region is commonly deconvoluted using multiple Gaussian sub-bands allowing for characterization of water structure under varying conditions.[20,50–52] Despite decades of research in this area, there is still much debate over the identity of the water assemblies that give rise to each sub-band.[20,21,50,52,53,57,61–64] For example, Sun and colleagues use five bands to fit the Raman O-H stretching band of bulk water. The bands are centered at 3041, 3220, 3430, 3572, and 3636 cm^{-1} and are assigned to the single donor-double acceptor (DAA), double donor-double acceptor (DDAA), single donor-single acceptor (DA), double donor-single acceptor (DDA), and free-OH water arrangements, respectively.[52,57] In contrast, studies of dilute water in ionic and dipolar liquids have deconvoluted the FTIR O-H stretching band into 3-5 Gaussians. These bands are assigned more generally to symmetrically and asymmetrically solvated water molecules as well as free-OH stretching. The absolute positions of these bands are dependent on the identity of the solvent.[20,21,29]

Herein we present, to the best of our knowledge, the first Raman and MD simulation study of the liquid structure of water-in-propylene carbonate mixtures. We evaluate the structure of dilute water in PC as the concentration is increased from $\chi_{water} = 0.003$ up to saturation ($\chi_{water} = 0.296$). Analysis of the O-H stretching, and carbonyl regions of the Raman spectra reveals a hydrogen bond structure that is distinctly different from bulk water and highly concentration dependent. The noncoincidence effect

(**NCE**) in the polarized carbonyl Raman band provides insight into structural changes in PC due to water solvation. Isotopic dilution spectroscopic experiments (10% HOD in D_2O) bridge the gap between experiment and simulations as well as highlight the extent of intramolecular vibrational coupling within water aggregates. Molecular dynamics simulation results find that water associates with itself in PC more than previous experimental inferences.[12,14] Our simulations also provide the first insight into the structure of water aggregates within PC and their compositional evolution. This study expands the fundamental knowledge of the behavior of limited water in complex solvation environments, which has applications in various fields including, materials and electrochemistry.

Methods

Materials and Sample Preparation

Solutions of dilute water dispersed in PC were prepared in the concentration range of $0.003 \leq \chi_{water} \leq 0.296$. These concentrations span the water-in-PC solubility range, stopping near the known miscibility gap ($0.33 \leq \chi_{water} \leq 0.95$ at 20 °C) of the two liquids.[14] PC/water solutions were prepared by the incremental addition of ultrapure water (Milli-Q Advantage A10, resistivity 18.2 MΩ) to 3.2626 ± 0.0017 g of PC (Sigma-Aldrich, ≥ 99.7%, anhydrous) in a standard quartz cuvette (Starna, 10 mm path length) that was sealed using a cap equipped with a silicone gasket to provide an air-tight seal. To limit water contamination of the solvent, a single-use sterile syringe and needle were used to transfer PC from the septum sealed bottle directly to the cuvette for immediate use without further purification. Thus, the purity of PC can be reasonably assumed to be that reported by the manufacturer (purity ≥ 99.65%, water content by Karl Fischer titration ≤ 0.002 %).[65] To further limit excess water in the system, the cuvette was dried in a 150 °C oven for at least 12 hours before use.

Prior to the addition of water, the Raman spectrum of the pure PC sample was acquired. To achieve the desired molar ratio, water was then added to the PC sample incrementally until phase

separation was reached. Phase separation occurred between a total of 240 and 260 μL of water added for all samples which corresponds to a water concentration in PC between χ_{water} = 0.29 and 0.31. The exact amount of water added to PC was determined by weighing the cuvette after each water addition (Mettler Toledo, XS104, ± 0.1 mg). Following each addition of water to PC, the sealed cuvette was manually shaken for at least 2 minutes then allowed to settle, undisturbed for 2 minutes prior to acquiring the polarized Raman spectra. Experiments were performed in duplicate at a room temperature of 20 °C.

Raman Spectroscopy

The custom-built Raman spectrometer used in the current work has been described previously.[66] Briefly, the Raman spectrometer consists of a diode-pumped continuous wave excitation laser (532 nm, 100:1 vertically (V) polarized, CrystaLaser) directly coupled to a Raman probe optical system (InPhotonics). Scattered light is collected using two independent fiber-optic cables which simultaneously collect the parallel (VV) and perpendicular (VH) polarized responses. The fiber optics are coupled to a spectrograph (IsoPlane 320, Princeton Instruments) using a 150 μm slit width and 600 g/mm grating (750 nm blaze). The two polarized signals are detected on separate regions of a LN_2-cooled CCD detector (Pylon 400BRX back-illuminated, Princeton Instruments). Spectra are collected by averaging 150 spectra using a 0.045 s exposure time. Laser power stability was ensured by taking the Raman spectrum of pure water following every 5 sample spectra. Intensity variations in the OH stretching region of the water spectrum were < 0.6% for all experiments.

Computational Studies

In order to validate the molecular inferences concerning the structure of water/PC mixtures, we developed a molecular dynamics simulation model. Using a GROMOS forcefield with an SPC/E water model, we simulated water/PC mixtures across a range of compositions between dilute solutions

and across the experimental miscibility gap.[67,68] All simulations were done under fixed number of molecules, temperature, and pressure using a Nose-Hoover thermostat and barostat.[69,70] The temperature and pressure were fixed to 298 K and 1 bar, respectfully. The number of molecules was equal to 200 PC molecules plus the number of water molecules necessary to fix the mole fraction between 0.04 and 0.22. Standard periodic boundary conditions, Ewald summation treatment of electrostatic interactions and a 2 fs timestep was employed in all simulations with the covalent hydrogen bonds held rigid with RATTLE.[71] Each composition was simulated for 10 ns, with an initial 1 ns simulation at elevated temperature of 400 K and fixed volume to equilibrate the initial composition fluctuations. The specific forcefields were choosen because of their previous validation in related studies. The specific water model SPC/E has been previously showns to provide an accurate model for the electrostatic environments contributing to the inhomogenious vibrational line shapes[72–74] and SPC/E GROMOS mixtures are able to reproduce experimental trends in solvation thermodynamics.[75]

Results and Discussion

It is well known that the liquid structure of water is highly sensitive to its environment, yet there is still much debate over the microscopic mechanisms that govern water structure, particularly within systems where water is the solute. The aim of this study was to utilize a combined computational and experimental Raman approach to determine how dilute water partitions and interacts within a propylene carbonate (PC) solvent environment as water is increased up to the saturation limit. Structural changes within PC induced by the addition of water were also evaluated.

Raman Spectroscopy

The polarized Raman spectra of PC solutions were acquired as the water concentration was increased from a mole ratio of $\chi_{water} = 0.003$ to the saturation point (phase-separation) at $\chi_{water} = 0.296$. Particular attention is paid to the O-H stretching (3000 – 3800 cm^{-1}) and carbonyl regions (1720 –

1820 cm^{-1}) to determine water structure. The O-H stretching region consists of a broad band resulting from the population distribution of hydrogen-bonded water assemblies, which are expected to evolve as more water is added to the system.[6,11,50,51] Deconvolution of the O-H stretching band into Gaussian sub-bands allowed for the characterization of water structure. The carbonyl band revealed interactions of water with the solvating environment and developed a complete picture of how the PC bulk structure evolves to accommodate the solvation of water molecules.

Water Structure

The O-H stretching region of the PC/water Raman spectra after removing spectral contributions of pure PC through pre-processing is depicted in Figure 1. Further discussion of the spectral pre-processing procedure is presented in the Electronic Supplemental Information (ESI, see also Figures S1 & S2). These results demonstrate that the O-H stretching band increases in intensity and broadness as the water concentration is increased. It is difficult to determine the solvation structure of water from these spectra without further deconvolution of the hydrogen bonded sub-structure, therefore a Gaussian fitting was applied to this region. The fitting procedure is described in the ESI and the converged parameters are included in Table S1 and Figure S3.

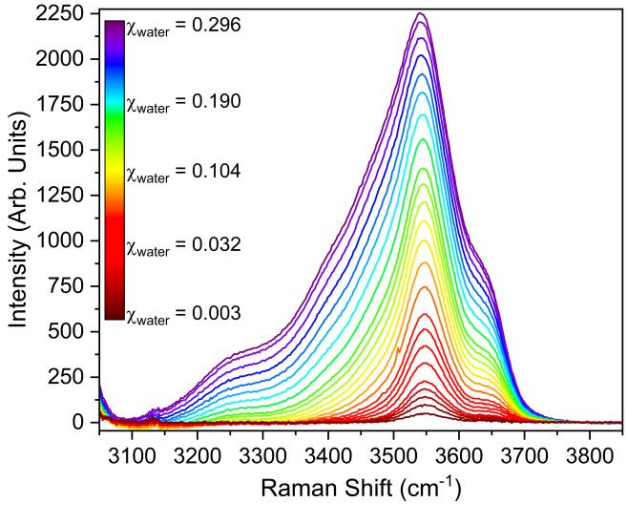

Figure 1. Raman spectra (VV polarization, O-H stretching region) of PC as water concentration is increased from 0.003 mole fraction (red) to 0.296 mole fraction (violet). Spectra demonstrate that O-H stretching band increases in intensity and broadness as water is added to PC.

The number of Gaussian bands required for the fit was dependent on water concentration. In the low water concentration spectra ($\chi_{water} < 0.091$), only three Gaussian bands are required for the fit. These bands are centered at approximately 3480, 3550, and 3643 cm^{-1}. A representative spectrum for the low water concentrations ($\chi_{water} = 0.013$) is plotted in Figure 2a. Based on literature of aqueous interfaces and confined water, the highest frequency Gaussian, centered at 3643 cm^{-1}, is assigned to dangling-OH groups (also referred to as "free-OH" in previous publications).[76–82] These O-H groups are pointed towards the solvating PC molecules, but are not participating in a hydrogen bond. The dangling-OH vibrational band arising from the hydration shells of dissolved nonpolar groups has been reported to occur at ~3660 cm^{-1}.[76,78] In our spectra, this band is shifted to lower energy due to the solvating dielectric environment.[20]

Based on previous water cluster and dilute water studies, the second and third Gaussians, which occur at ~3550 and 3480 cm^{-1}, respectively, are assigned to "partially coordinated" water species.[14,29,52,83,84] The water molecules that make up these groups form between one and three hydrogen bonds, but still do not form the fully coordinated, tetrahedral structure.[14,52] The partially coordinated water population can be further classified based on the degree of hydrogen bonding.[57,76,83,85] Evidence for this is provided by Suhm and coworkers who assigned the 3550 and ~3430 cm^{-1} bands in the FTIR spectrum of thermally excited water clusters to the trimer and tetramer water species, respectively.[83] Similar band positions were observed by Dei and Grassi in the FTIR spectra of dilute water in PC. The band observed at 3570 cm^{-1} was assigned to "multimer water" that is weakly connected to its environment. Additionally, they assigned the band centered at 3450 cm^{-1} to "intermediate water" that is moderately coordinated to other water molecules, but still has distorted hydrogen bonds.[14] Based on these studies, it is clear that the band we observe at 3550 cm^{-1} results from water molecules with low coordination and the band we observe at 3480 cm^{-1} results from water that is more coordinated in comparison. Therefore, we refer to the 3550 and 3480 cm^{-1} band

populations as "low coordination" and "moderate coordination" water, respectively. Here, we choose to use broad language to describe the two center sub-bands to avoid speculating on the types of water aggregates formed in PC, which we cannot determine with spectra alone. These aggregates will be further explored using MD simulations.

Beginning at χ_{water} = 0.091 up to the saturation point, a fourth Gaussian is needed for the fit. The final and lowest frequency band is centered at ~3260 cm^{-1}. Based on well-established literature of bulk water and clusters, this band is assigned to water that forms four hydrogen bonds in an approximately tetrahedral geometry.[11,52] In water clusters, this peak is only observed for hexamers or larger cluster sizes.[83] To align with our chosen terminology, we refer to this population as "full coordination" water. The full coordination water band can be observed in Figure 2b, where a representative spectrum for the high water concentrations (χ_{water} = 0.232) is plotted.

To validate the peak assignments for the deconvoluted OH-stretching sub-bands, we considered the extent of intermolecular vibrational coupling for each of the sub-bands. This was achieved through isotopic dilution, where 5% H_2O in D_2O (10% HOD) was added incrementally to PC instead of pure water. As a result, the O-H stretching mode is decoupled and can be used as a more accurate reporter of water structure.[61] The spectra of dilute O-H in PC/D_2O mixtures was deconvoluted in the same manner as the PC/H_2O spectra and the results are plotted in Figure S4. To estimate the relative degree of vibrational coupling for each water assembly observed, the intensity ratio of each sub-band to the highest intensity sub-band (low coordination, ~3550 cm^{-1}) is compared before and after decoupling at a constant water concentration. In the PC/H_2O spectrum, the intensity ratios for the moderate coordination at ~3480 cm^{-1} and dangling-OH band at 3643 cm^{-1} are 1.02 and 0.38, respectively. In the decoupled spectrum, these ratios are 0.58 and 0.33, respectively. Upon removal of vibrational coupling, the relative intensity of the moderate coordination water compared to the low coordination decreases significantly whereas the relative intensity for the dangling-OH

decreases only slightly. This demonstrates that the water assembly responsible for the band at ~3480 cm^{-1} experiences more intermolecular vibrational coupling and is therefore more coordinated than those giving rise to either the ~3550 cm^{-1} or the 3643 cm^{-1} bands. Thus, our peak assignments of increasing water coordination with decreasing frequency are supported. The intensity ratio for the 3260 cm^{-1} band in the PC/H_2O spectrum is 0.18. This band did not have enough intensity in the decoupled spectrum to be resolved from the PC band at 3220 cm^{-1}, so an intensity ratio was not able to be obtained. However, the lack of intensity for this band in the decoupled spectrum indicates that this assembly does experience some degree of coupling and further supports our assignment.

Comparison of the low (Figure 2a) and high (Figure 2b) water concentration deconvolutions reveals that the largest spectral changes due to increasing water concentration occur for the moderate and full coordination water species. The fully coordinated water peak, which is initially not present, is observed as water is added to the system. The moderate coordination water peak significantly increases in broadness and intensity, accounting for much of the changes observed in the entire O-H stretching region. The same trends were observed when the ATR-FTIR spectra of the PC/water mixtures, taken to supplement the Raman data, were deconvoluted in the same manner (see Figures S5 and S6).

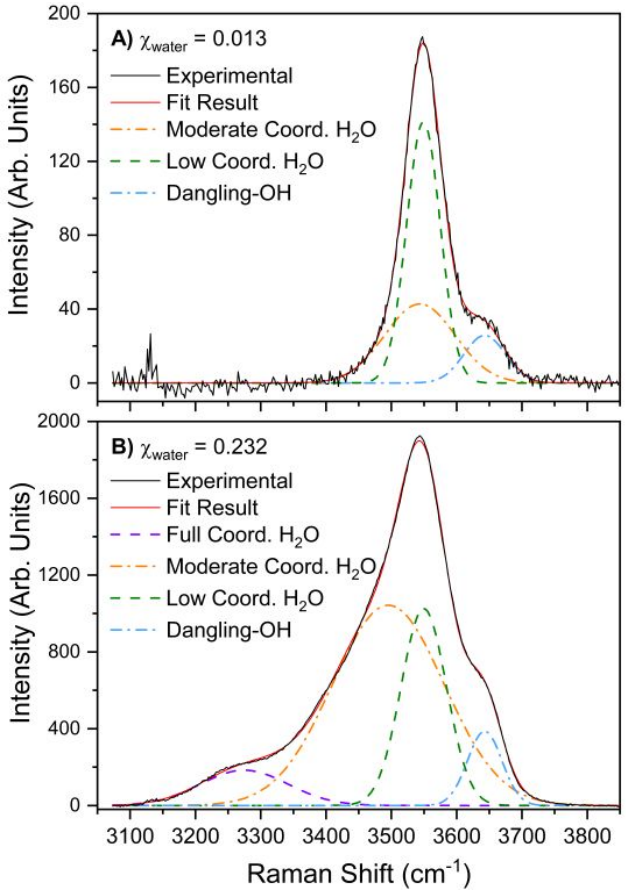

Figure 2. Gaussian deconvolution of experimental Raman O-H region for water concentrations χ_{water} = 0.013 (A) and 0.232 (B). Experimental (black) and fit (red) spectra are plotted with solid lines. Dashed lines represent Gaussian bands used to fit experimental spectra. Comparison of (A) and (B) reveals that the full coordination H_2O arrangement does not occur in PC when $\chi_{water} < 0.091$.

Analysis of the individual deconvoluted Raman bands as a function of water concentration (Figure 3) allowed for further understanding of how the water structure in PC evolves. Upon the addition of water, the full coordination band (Figure 3a) increases in intensity and shifts significantly ($\Delta\nu = -70$ cm^{-1}) to lower frequencies (red-shifts). Similarly, the moderate coordination band (Figure 3b) increases in intensity and red-shifts ($\Delta\nu = -53$ cm^{-1}). The shifting of vibrational bands to lower frequency as a function of concentration is attributed to the strengthening of hydrogen bonds or other intermolecular interactions with the oscillator. Moreover, the O-H stretching region in Raman spectra

has been shown to be sensitive to the degree of tetrahedral order within water, where the band shifts strongly to lower frequencies as the tetrahedral order is increased.[86] The observed red-shifts in the moderate and full coordination bands are consistent with the formation of ordered hydrogen bond configurations which have increasing tetrahedral character and stronger bonds.

The low coordination (Figure 3c) and dangling-OH (Figure 3d) bands behave similarly as the water concentration is increased. Both bands increase in intensity as a result of an increase in the total water molecules in the system. These Gaussian bands also do not undergo strong frequency shifts. The low coordination band increases in frequency (blue-shifts) by a total of 2 cm^{-1}. This can be attributed to intrinsic error in the fitting analysis or could be indicative of subtle weakening of the hydrogen bonds for this species. The frequency of the dangling-OH band did not change appreciably between the highest and lowest water concentration studied; therefore, it was held constant for all subsequent fittings (see ESI). The fact that the peak positions of the low coordination and dangling-OH bands do not change appreciably indicates that the water species that make up these populations do not undergo significant structural changes as the water concentration is increased.

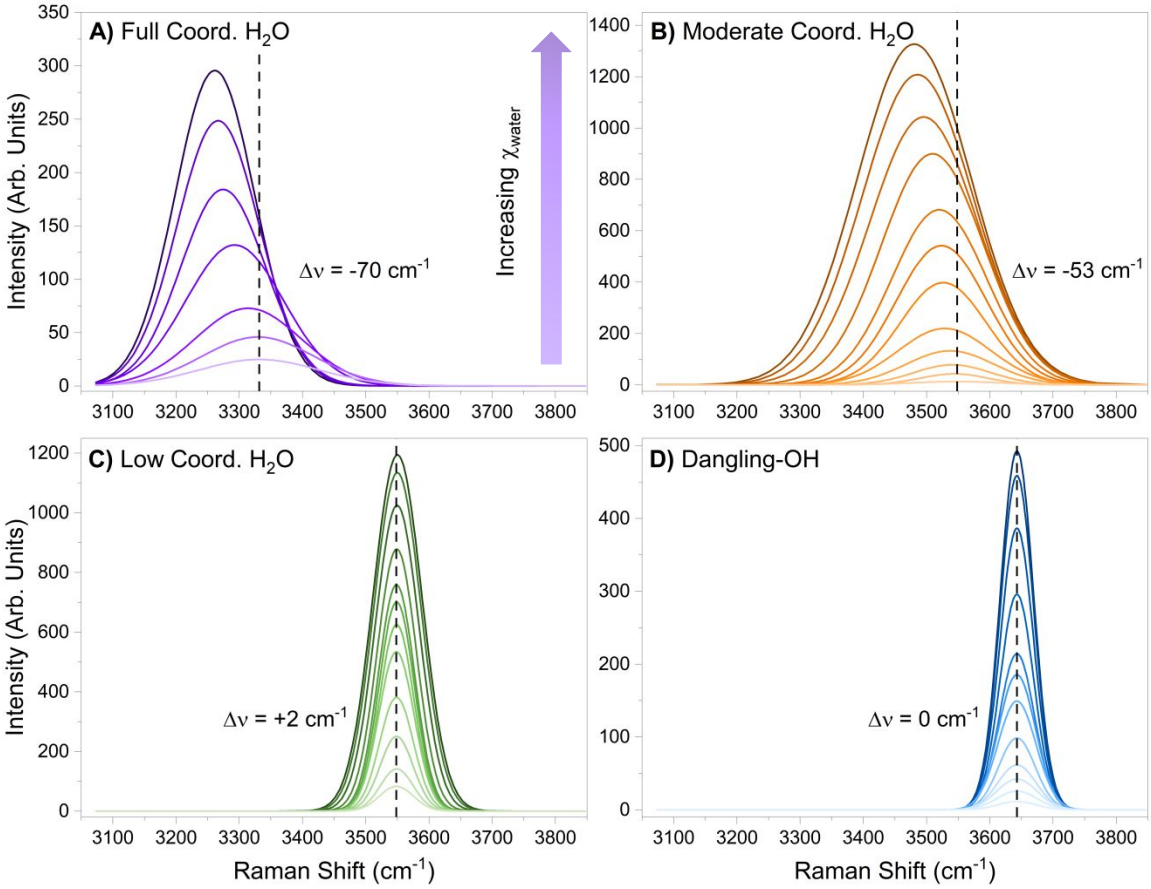

Figure 3. Evolution of the deconvoluted Gaussian bands as the water concentration in PC is increased. Each band corresponds to a different hydrogen bonded population of water; full coordination (A, violet), moderate coordination (B, orange), low coordination (C, green), and dangling-OH (D, blue). Darker colors correspond to higher water concentrations and dashed reference lines are set at peak position for lowest water concentration. The moderate and full H_2O bands undergo the largest peak shifts as the water concentration in PC is increased.

The present analysis of the Raman O-H stretching region assumes that water exists within one of four populations based on its hydrogen bonding state: dangling-OH, low coordination, moderate coordination, or full coordination. The O-H transition moment strength is assumed to remain constant across the individual solutions, therefore it follows that the total area of the O-H stretching band is the sum of the areas of the deconvoluted bands attributed to the different water population. Taking this into account, we calculated the percent of the total area taken up by the individual water populations as a function of water concentration. In Figure 4, the percent of the total O-H stretching area taken up by each Gaussian is plotted as a function of water mole fraction. This plot demonstrates how the relative concentration of the water populations change as water is added to PC.

At the lowest water concentrations in PC, the low coordination population is present in the highest relative concentration. As water is added, the concentration of the low coordination state decreases sharply and levels off around χ_{water} = 0.20 with a total decrease of 41%. Correspondingly, the moderate coordination population sharply increases in relative concentration as water is added. The total increase in the contribution of this band is 34%. The inverse trend in the relative concentration of the low and moderate coordination states demonstrates a shift in hydrogen bond structure as water is added to PC. Under very dilute conditions, water molecules exist primarily in low coordination states and do not interact strongly with one another. As water concentration is increased, water structure shifts and a greater population of water exists in moderate and full coordination states. The leveling off of the relative concentration curves in Figure 4 indicates that this shift in structure is complete at χ_{water} = 0.20.

The full coordination and dangling-OH populations do not experience significant changes in relative concentration. The full coordination state is not present until χ_{water} = 0.091 is reached due to the low intensity of this band at more dilute concentrations. This band undergoes an overall relative concentration increase of 9%, which indicates that a larger fraction of the total water molecules exists in the most coordinated, tetrahedral state. This is only possible if water is interacting strongly with itself and forming aggregates larger than hexamers.[20] The relative concentration of the dangling-OH population remains approximately constant at 8%. This concentration of dangling-OH is higher than in bulk water where it is ~3%.[52] We conclude that the solvating PC environment yields a water hydrogen bonding structure that is disrupted from typical bulk water organization. Instead, PC supports a higher concentration of dangling-OH groups.

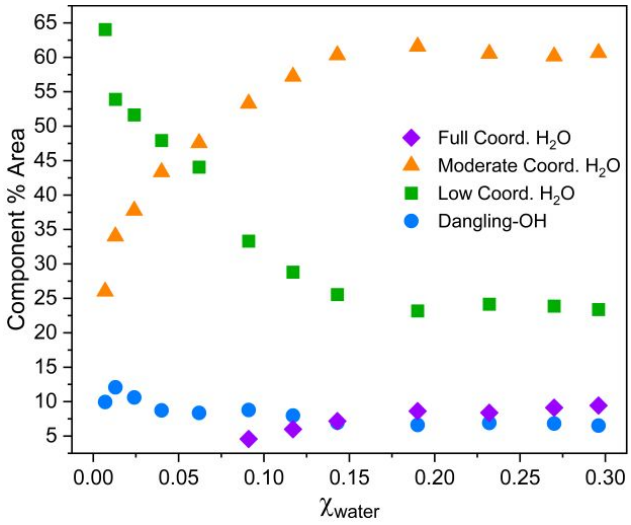

Figure 4. Percent of the total O-H stretching area taken up by each Gaussian band as a function of water concentration. When analyzing a single water concentration, the component % area of each sub-band can be interpreted as the relative concentration of each water arrangement.

Based on the observed changes to the hydrogen-bonded sub-structure, we conclude that at low concentrations of water in PC, water does not self-associate to an appreciable extent. Instead, it is primarily solvated by weaker intermolecular interactions with PC. The presence of the 3480 and 3550 cm^{-1} bands at the lowest water concentration spectra suggest that a fraction of water molecules in PC form small aggregates such as dimers up to potentially tetramers and pentamers. We also conclude that concentrations above χ_{water} = 0.091, water self-associates to a greater extent, forming relatively large aggregates within the PC environment. The presence of the fully coordinated water peak indicates that a significant portion of clusters formed have increasing tetrahedral order and must be hexamers or larger. In contrast to previous conculsions,[12,14] we observe a gradual transition from mostly solvated water molecules to primarily aggregated water molecules in PC.

Using molecular dynamics (**MD**) simulations, we have quantified the degree of water clustering in PC by computing the average number of hydrogen bonds between water molecules as a function of bulk composition. Example snapshots from the MD simulations are shown in Figure 5a.

These characteristic configurations show that water is well dispersed in the majority PC fluid. To accomplish this, we have employed a geometric criteria from Luzar and Chandler[87] for defining a hydrogen bond (n_{HB}) as an oxygen-oxygen separation distance of less then 3.5 Å and an angle between the oxygen-oxygen displacement vector and the oxygen-hydrogen bond vector as less then 30°. The results of these calculations are shown in Figure 5b where we enumerate the probability $P(n_{HB})$ of both the number and type of hydrogen bond. Specifically, we have differentiated molecules that are double hydrogen bond donors (DD), double acceptors (AA), single acceptor-single donors (DA), or double-donor single acceptors (DDA). At χ_{water} = 0.04, water exists as a monomer 70% of the time, with the probability of dimers and trimers falling along Poisson statisics. At elevated water concentrations, the mostly likely structure becomes chains of water molecules each with two hydrogen bonds, one donated and the other accepting. The number of three and four coordinated water remains low, totalling only a combined 25% of solubilized water at the highest mole fractions considered, χ_{water} = 0.22. These basic trends agree qualitatively with those in Figure 4 from the Gaussian deconvolution of the experimental Raman spectra.

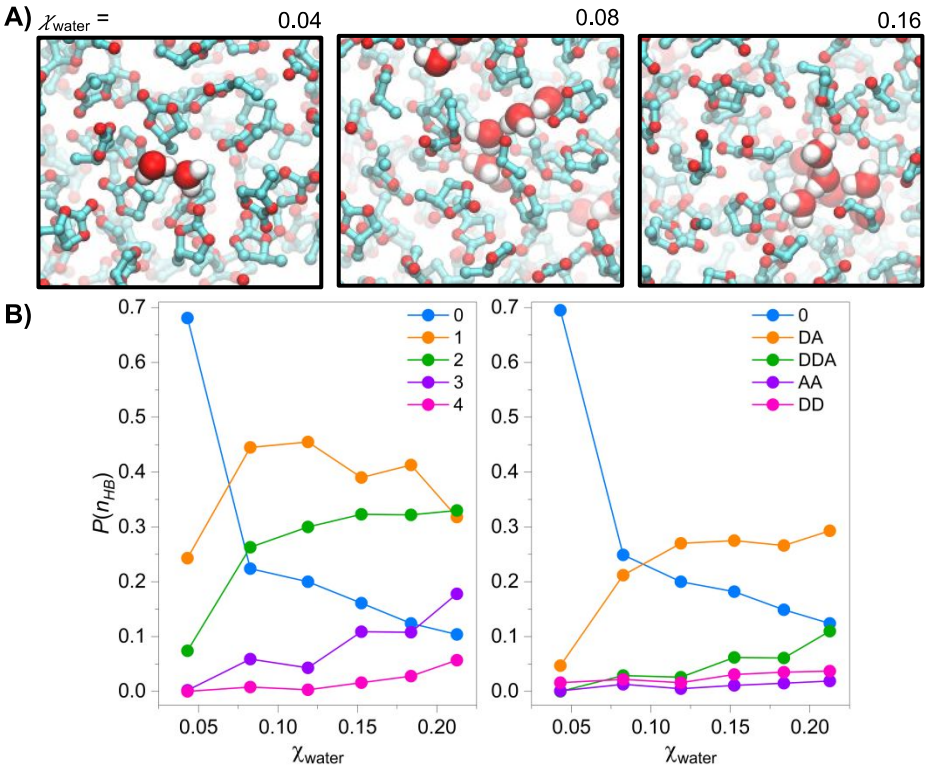

Figure 5. Molecular dynamic simulations of water-PC mixtures. A) Characteristic snapshots at different compositions. B) Probability of different hydrogen bond arrangements. Results demonstrate that water associates with itself to a greater extent at higher concentrations.

As inferred from the experimentally deconvolved Raman spectra, the simulations confirm that the O-H stretching frequency is determined by a large extent to the degree of hydrogen bonding between water molecules. To calculate the Raman spectra, we have employed a frequency map based approach.[60] Specifically, in the purely inhomogeneous broadening limit, the Raman lineshape is a probe of the local electric field, ξ along the OH bond vector.[88] This follows from the a Stark effect and first order perturbation theory between the oscillator and the surrounding bath such that the frequency shifts are given by $\omega - \omega_o = Q\xi$, where ω_o and Q are taken here as empirical parameters determined to best fit the lineshape. Specifically, a proceedure that has been employed by Geissler and coworkers in pure water and aqueous solutions, is to map the Raman lineshape to the distribution of electric fields acting on the hydrogen in the direction of the OH bond vector.[73] To validate this approach, we have plotted in Figure 6a the distribution of electric fields on top of the experimentally

measured O-H stretching region of the Raman lineshape for diluted HOD in D_2O/PC mixtures. Using diluted HOD in D_2O, allows us to decouple the oscillators, and mitigate effects from delocalization of the vibrations.[61,72,89,90] As observed in past simulations,[74] this simple classical perspective on the Raman lineshape allows us to identify specific molecular structures that give rise to features in the relatively broad lineshape.

The simulation and experimental lineshape for dilute HOD match well over the compositions considered, with an asymmetric shape rising quickly at high fequencies and falling slowly at low frquencies. Notably sharp features in the H_2O in PC lineshape at 3250 cm^{-1} and 3650 cm^{-1} are less pronouced in the diluted HOD spectra and the corresponding simulations, suggesting that some of the structure results from delocalization of the oscillation. Upon increasing the concentration of water, the simulated spectra from the mapped frequencies in Figure 6b show the same basic trends as those observed experimentally, namely an increased broadening in the form of a lower frequency or, equivalently, a larger magnitude electric field. In the simulations, this growing mode at lower frequency is identified as the O-H oscillator donating a hydrogen bond to another water molecule. No other motif strongly correlates with the increasing intensity, as only local hydrogen bonding produces such drammatically different local electric fields (see Figure S8).

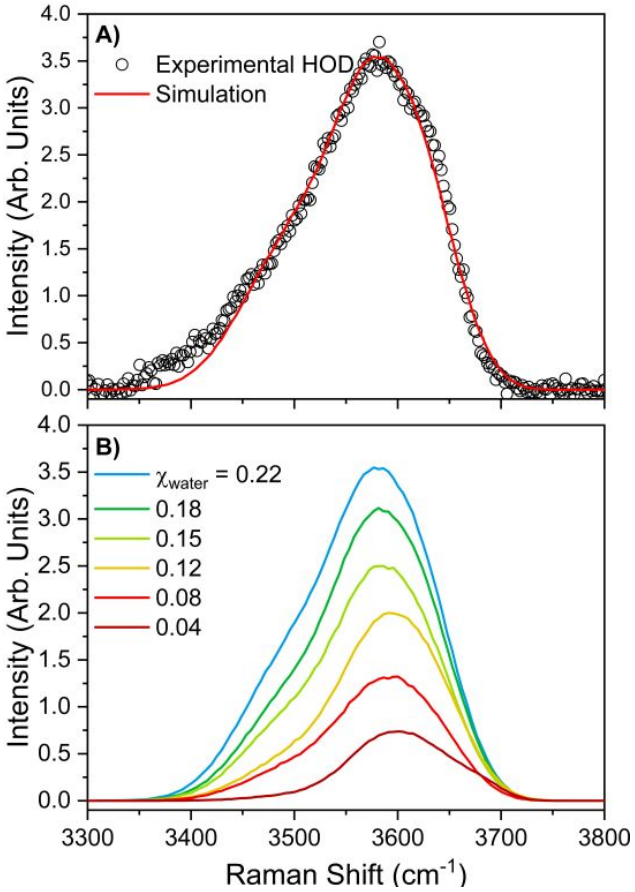

Figure 6. Raman spectra (O-H stretching region) from molecular dynamics simulations of dilute HOD. A) Comparison of experimental spectra and frequency mapped spectra for 0.22 mole fraction. B) Simulated spectra as water concentration is increased from 0.04 mole fraction (red) to 0.22 mole fraction (blue).

Propylene Carbonate Structure

To gain insight into the effect that the addition of water has on the bulk structure of PC, the carbonyl region of the experimental and theoretical spectra were analyzed. The experimental carbonyl stretch Raman spectra as a function of water concentration are presented in Figure 7 with the theoretical spectra plotted in the inset. The carbonyl peak for pure PC has been reported to occur in the Raman spectrum at approx. 1780 cm^{-1}, with a Fermi resonance band causing a shoulder on the high-frequency side.[33,37,91] Here, we observe the carbonyl band for pure PC at 1779 cm^{-1}, where it undergoes a small red-shift ($\Delta\nu$ = ~2 cm^{-1}) and an overall decrease in intensity as the concentration

of water is increased (Figure 7). The decrease in intensity of the band is a result of the dilution of PC that occurs upon each addition of water. As described above, the red-shift that this band undergoes is indicative of strengthening intermolecular interactions with the oscillator. The carbonyl band in vibrational spectra has previously proven to be a sensitive probe for hydration structure, producing significant shifts (upwards of $\Delta\nu$ = 20-30 cm^{-1}) upon changes in hydration.[92–94] As a result, we assert that the water concentration-dependent red-shift of the carbonyl band is due to the formation of weak water-PC hydrogen bonding at this molecular site. These are in agreement with the MD simulations, where the C=O stretch is computed in an analogous manner as those of the O-H stretch in water, using the electric field acting in the direction of the C=O bond vector.

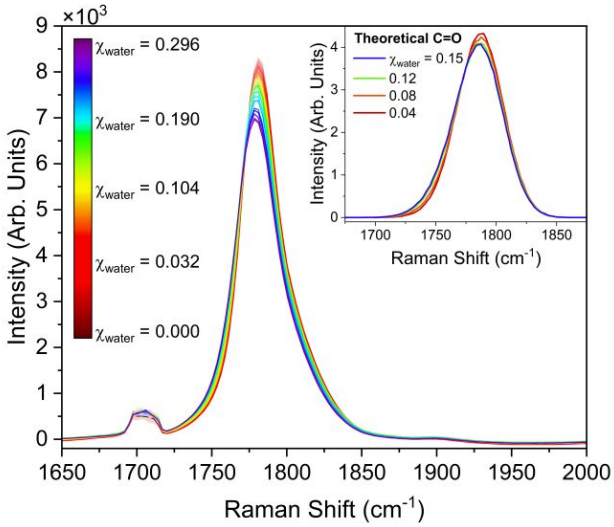

Figure 7. Raman spectra (VV polarization, carbonyl stretching region) of PC as water concentration is increased from χ_{water} = 0 (red) to 0.296 (violet). Band structure occurring at ~1710 cm^{-1} is a result of an artifact in the Raman optical system and does not correspond to molecular vibrations. Theoretical C=O stretching spectra are plotted in the inset.

Further information on structural changes in PC can be gained through consideration of the polarized Raman spectra in terms of the noncoincidence effect (**NCE**). The noncoincidence effect refers to the frequency difference between the isotropic and anisotropic components of a polarized Raman band ($\nu_{NCE} \equiv \nu_{isotropic} - \nu_{anisotropic}$), which originates from resonant vibrational energy transfer

between molecules that are intermolecularly coupled (e.g. by hydrogen bonds, permanent dipole moments, etc.).[54,95–98] Coupling between dipoles in pure propylene carbonate produces a relatively large and positive NCE in the carbonyl band, typically ~10 cm^{-1}.[33,97] In prior studies by the Allen lab and others, the NCE has been used to determine structural organization changes in dipolar liquids due to ion solvation.[33,66,95,96,99] For example, Giorgini and coworkers demonstrated that the addition of mono- and divalent cation salts to acetone produced large, negative carbonyl NCEs due to solvent clustering around the cation.[95,99]

In this study, we have calculated the isotropic (I_{iso}) and anisotropic (I_{ansio}) components of the carbonyl stretching band using the VV and VH polarized Raman spectra and the following equations: $I_{iso} = I_{VV} - \frac{4}{3}I_{VH}$ and $I_{aniso} = \frac{4}{3}I_{VH}$.[54] In Figure 8, the carbonyl band NCE resulting from pure PC (Figure 8a) and from the PC solution with the maximum water concentration, χ_{water} = 0.296, (Figure 8b) are compared. The addition of water to PC causes a total NCE decrease of 0.5 cm^{-1}, which is consistent with the formation of weak hydrogen bonds between the carbonyl of PC and water.[96] The observed change in NCE as water is added to PC is small in comparison to previously reported carbonyl NCE changes in propylene carbonate as well as in other similar solvents.[33,91,99] Thus, we conclude that the bulk structure of PC is not significantly perturbed by the addition of water up to the solubility limit.

The symmetric and asymmetric ester stretching bands were also analyzed to provide additional information on bulk PC liquid structure as a function of water concentration. The polarized and depolarized Raman response of the ester bands is plotted in Figure S7. We find that the addition of water to PC causes a small blue-shift for both ester bands where $\Delta\nu$ is 0.50 and 0.42 cm^{-1} for the symmetric and asymmetric bands, respectively. This shift likely indicates a slight weakening of ester intermolecular forces as water is added, which supports the conclusion that the PC-water interaction occurs primarily at the carbonyl site and not the ester oxygens. Analysis of the NCE for the ester

bands also supports this conclusion. The NCE for both ester bands remains relatively unchanged from the pure PC spectrum to the highest water concentration spectrum, only changing by < 0.08 cm^{-1}. Based on our analysis of the polarized Raman response of PC molecules as a function of water concentration, we conclude that the carbonyl is the primary site of interaction with water and that this interaction does not cause the bulk PC liquid structure to rearrange to accommodate water solvation.

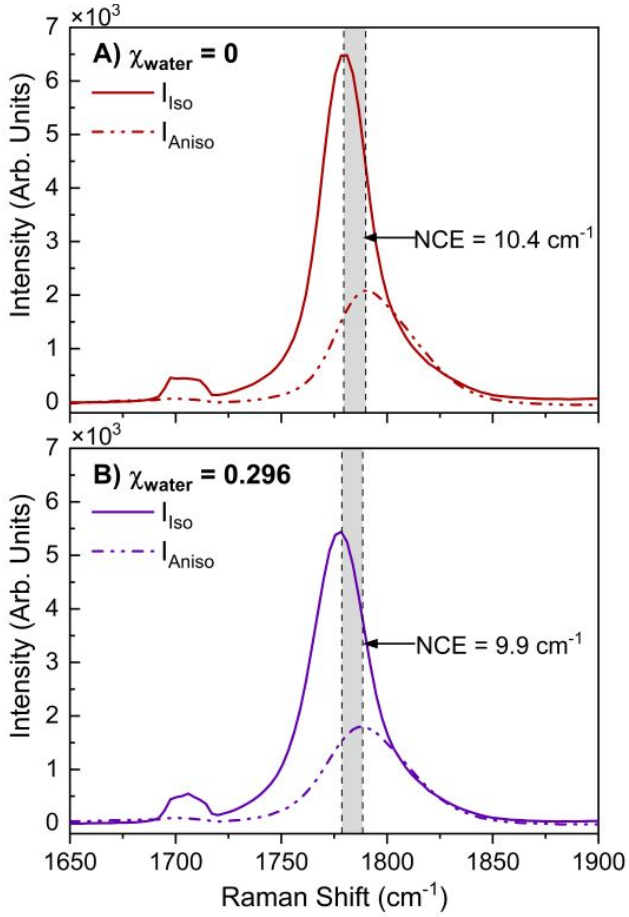

Figure 8. Isotropic (solid line) and anisotropic (dashed line) components of the polarized carbonyl Raman band for pure PC (A, red) and PC with water added to a mole fraction of 0.296 (B, violet). Dashed reference lines are included at the carbonyl peak position (determined by Gaussian fitting) for the isotropic and anisotropic components. The shaded gray area represents the noncoincidence effect (difference in isotropic and anisotropic peak positions) for each solution.

Conclusions

In this work, we characterize water concentration-dependent structural changes of a PC/water binary system using polarized Raman spectroscopy and molecular dynamics simulations. Gaussian deconvolution of the OH region in the experimental spectra reveals a water hydrogen-bond structure that consists of either three or four sub-bands that are assigned based on the degree of hydrogen bonding. For water concentrations in PC less than $\chi_{water} = 0.091$, dangling-OH, low coordination, and moderate coordination states are observed. Above this concentration, a fourth sub-band is observed, which corresponds to fully coordinated, tetrahedral water. As evidenced by the evolution of the water hydrogen bond sub-bands, water is primarily solvated by PC under dilute conditions and does not tend to form aggregates. Increasing the water concentration leads to an increase in tetrahedral water structure and indicates that water exists primarily in aggregates at higher concentrations. MD simulation results support this conclusion as well as provide additional insight into the size and type of aggregates formed. Simulations of the system where $\chi_{water} = 0.04$ reveal that water exists as monomers 70% of the time, with dimers and trimers accounting for the remaining conformations. Interestingly, the simulations find that the mostly likely water structure at elevated concentrations is chains of water molecules, each with two hydrogen bonds. Experimental and simulation results show that the hydrogen bond structure of water is distinctly different from the bulk at all concentrations, where the presence of three and four coordinate water is lower and dangling-OH is higher in comparison to bulk. The bulk structure of PC is not significantly perturbed by the addition of water as demonstrated by a change in carbonyl NCE of only 0.5 cm^{-1} from pure PC to the highest water concentration in PC. Overall, the addition of water to PC results in a relatively unperturbed PC structure, yet water structure evolves in a highly concentration-dependent manner. This yields a distribution of hydrogen bonded states including linear chains as well as structures with more tetrahedral local order.

Supporting Information

Contents: Raman spectra of the O-H stretching region prior to spectral pre-processing along with discussion of the pre-processing method, details of Gaussian fitting procedure for the O-H stretching region and a compilation of all converged fit parameters, Deconvoluted HOD spectra for peak assignments, ATR-FTIR spectra of a subset of PC/water solutions, analysis of the ester stretching bands in the Raman spectra, and explanation of the electric field fluctuation decomposition applied to calculated Raman spectra.

Acknowledgements

The authors acknowledge support from the National Science Foundation through grant No. CHE-2102313. J.B.C. would like to thank A. Enders for insightful comments on the manuscript. The authors declare no competing financial interest.

References

(1) Ball, P. Water — an Enduring Mystery. *Nature* **2008**, *452* (7185), 291–292. https://doi.org/10.1038/452291a.
(2) Nilsson, A.; Pettersson, L. G. M. The Structural Origin of Anomalous Properties of Liquid Water. *Nat. Commun.* **2015**, *6* (1), 8998. https://doi.org/10.1038/ncomms9998.
(3) Fayer, M. D.; Levinger, N. E. Analysis of Water in Confined Geometries and at Interfaces. *Annu. Rev. Anal. Chem.* **2010**, *3* (1), 89–107. https://doi.org/10.1146/annurev-anchem-070109-103410.
(4) Corti, H. R.; Appignanesi, G. A.; Barbosa, M. C.; Bordin, J. R.; Calero, C.; Camisasca, G.; Elola, M. D.; Franzese, G.; Gallo, P.; Hassanali, A.; Huang, K.; Laria, D.; Menéndez, C. A.; de Oca, J. M. M.; Longinotti, M. P.; Rodriguez, J.; Rovere, M.; Scherlis, D.; Szleifer, I. Structure and Dynamics of Nanoconfined Water and Aqueous Solutions. *Eur. Phys. J. E* **2021**, *44* (11), 136. https://doi.org/10.1140/epje/s10189-021-00136-4.
(5) Shultz, M. J.; Baldelli, S.; Schnitzer, C.; Simonelli, D. Water Confined at the Liquid-Air Interface. In *Water in Confining Geometries*; Buch, V., Devlin, J. P., Eds.; Springer Series in Cluster Physics; Springer: Berlin, Heidelberg, 2003; pp 249–273. https://doi.org/10.1007/978-3-662-05231-0_12.
(6) Plastinin, I. V.; Burikov, S. A.; Dolenko, T. A. Laser Diagnostics of Reverse Microemulsions: Influence of the Size and Shape of Reverse Micelles on the Raman Spectrum on the Example of Water/AOT/Cyclohexane System. *J. Mol. Liq.* **2021**, *325*, 115153. https://doi.org/10.1016/j.molliq.2020.115153.
(7) Agrawal, K. V.; Shimizu, S.; Drahushuk, L. W.; Kilcoyne, D.; Strano, M. S. Observation of Extreme Phase Transition Temperatures of Water Confined inside Isolated Carbon Nanotubes. *Nat. Nanotechnol.* **2017**, *12* (3), 267–273. https://doi.org/10.1038/nnano.2016.254.

(8) Ma, X.; Cambré, S.; Wenseleers, W.; Doorn, S. K.; Htoon, H. Quasiphase Transition in a Single File of Water Molecules Encapsulated in (6,5) Carbon Nanotubes Observed by Temperature-Dependent Photoluminescence Spectroscopy. *Phys. Rev. Lett.* **2017**, *118* (2), 027402. https://doi.org/10.1103/PhysRevLett.118.027402.
(9) Rieth, A. J.; Hunter, K. M.; Dincă, M.; Paesani, F. Hydrogen Bonding Structure of Confined Water Templated by a Metal-Organic Framework with Open Metal Sites. *Nat. Commun.* **2019**, *10* (1), 4771. https://doi.org/10.1038/s41467-019-12751-z.
(10) Hunter, K. M.; Wagner, J. C.; Kalaj, M.; Cohen, S. M.; Xiong, W.; Paesani, F. Simulation Meets Experiment: Unraveling the Properties of Water in Metal–Organic Frameworks through Vibrational Spectroscopy. *J. Phys. Chem. C* **2021**, *125* (22), 12451–12460. https://doi.org/10.1021/acs.jpcc.1c03145.
(11) Crupi, V.; Interdonato, S.; Longo, F.; Majolino, D.; Migliardo, P.; Venuti, V. A New Insight on the Hydrogen Bonding Structures of Nanoconfined Water: A Raman Study. *J. Raman Spectrosc.* **2008**, *39* (2), 244–249. https://doi.org/10.1002/jrs.1857.
(12) Cogley, D. R.; Falk, M.; Butler, J. N.; Grunwald, E. Solvation and Self-Association of Water in Propylene Carbonate. *J. Phys. Chem.* **1972**, *76* (6), 855–864. https://doi.org/10.1021/j100650a011.
(13) Scherer, J. R.; Go, M. K.; Kint, S. Raman Spectra and Structure of Water in Dimethyl Sulfoxide. *J. Phys. Chem.* **1973**, *77* (17), 2108–2117. https://doi.org/10.1021/j100636a016.
(14) Dei, L.; Grassi, S. Peculiar Properties of Water as Solute. *J. Phys. Chem. B* **2006**, *110* (24), 12191–12197. https://doi.org/10.1021/jp060633l.
(15) Silva, P. L.; Bastos, E. L.; El Seoud, O. A. Solvation in Binary Mixtures of Water and Polar Aprotic Solvents: Theoretical Calculations of the Concentrations of Solvent−Water Hydrogen-Bonded Species and Application to Thermosolvatochromism of Polarity Probes. *J. Phys. Chem. B* **2007**, *111* (22), 6173–6180. https://doi.org/10.1021/jp068596l.
(16) Abe, H.; Yoshiichi, Y.; Hirano, T.; Ohkubo, T.; Kishimura, H. Hydrogen Bonding of Nanoconfined Water in Ionic Liquids. *J. Mol. Liq.* **2022**, 120383. https://doi.org/10.1016/j.molliq.2022.120383.
(17) Abe, H.; Takekiyo, T.; Yoshimura, Y.; Shimizu, A. Static and Dynamic Properties of Nano-Confined Water in Room-Temperature Ionic Liquids. *J. Mol. Liq.* **2019**, *290*, 111216. https://doi.org/10.1016/j.molliq.2019.111216.
(18) Yoshimura, Y.; Mori, T.; Kaneko, K.; Nogami, K.; Takekiyo, T.; Masuda, Y.; Shimizu, A. Confirmation of Local Water Structure Confined in Ionic Liquids Using H/D Exchange. *J. Mol. Liq.* **2019**, *286*, 110874. https://doi.org/10.1016/j.molliq.2019.04.151.
(19) Zhang, Z.; Zhang, Y.; Du, B.; Peng, Z. Liquid-like Poly(Ionic Liquid) as Electrolyte for Thermally Stable Lithium-Ion Battery. *ACS Omega* **2018**, *3* (9), 10564–10571. https://doi.org/10.1021/acsomega.8b01539.
(20) Mukherjee, K.; Palchowdhury, S.; Maroncelli, M. OH Stretching and Libration Bands of Solitary Water in Ionic Liquids and Dipolar Solvents Share a Single Dependence on Solvent Polarity. *J. Phys. Chem. B* **2022**, *126* (24), 4584–4598. https://doi.org/10.1021/acs.jpcb.2c02445.
(21) Palchowdhury, S.; Mukherjee, K.; Maroncelli, M. Rapid Water Dynamics Structures the OH-Stretching Spectra of Solitary Water in Ionic Liquids and Dipolar Solvents. *J. Chem. Phys.* **2022**, *157* (8), 084502. https://doi.org/10.1063/5.0107348.
(22) Zhong, X.; Fan, Z.; Liu, Z.; Cao, D. Local Structure Evolution and Its Connection to Thermodynamic and Transport Properties of 1-Butyl-3-Methylimidazolium Tetrafluoroborate

and Water Mixtures by Molecular Dynamics Simulations. *J. Phys. Chem. B* **2012**, *116* (10), 3249–3263. https://doi.org/10.1021/jp3001543.
(23) Hayes, R.; Imberti, S.; Warr, G. G.; Atkin, R. How Water Dissolves in Protic Ionic Liquids. *Angew. Chem. Int. Ed.* **2012**, *51* (30), 7468–7471. https://doi.org/10.1002/anie.201201973.
(24) Dickens, B.; Dickens, S. H. Estimation of Concentration and Bonding Environment of Water Dissolved in Common Solvents Using Near Infrared Absorptivity. *J. Res. Natl. Inst. Stand. Technol.* **1999**, *104* (2), 173–183.
(25) Ivanov, E. V.; Lebedeva, E. Yu. Volumetric Properties of H2O and D2O Solutions in Propylene Carbonate at T=(278.15, 288.15, 298.15, 308.15, and 318.15) K under Atmospheric Pressure. *J. Mol. Liq.* **2011**, *159* (2), 124–131. https://doi.org/10.1016/j.molliq.2010.12.009.
(26) Bonner, O. D.; Choi, Y. S. Hydrogen Bonding of Water in Organic Solvents. II. Change of Water Structure with Composition. *J. Phys. Chem.* **1974**, *78* (17), 1727–1731. https://doi.org/10.1021/j100610a010.
(27) Johnson, J. R.; Christian, S. D.; Affsprung, H. E. The Molecular Complexity of Water in Organic Solvents. Part III. *J. Chem. Soc. Inorg. Phys. Theor.* **1967**, No. 0, 1924–1928. https://doi.org/10.1039/J19670001924.
(28) Christian, S. D.; Taha, A. A.; Gash, B. W. Molecular Complexes of Water in Organic Solvents and in the Vapour Phase. *Q. Rev. Chem. Soc.* **1970**, *24* (1), 20. https://doi.org/10.1039/qr9702400020.
(29) Glew, D. N.; Rath, N. S. H2O, HDO, and CH3OH Infrared Spectra and Correlation with Solvent Basicity and Hydrogen Bonding. *Can. J. Chem.* **1971**, *49* (6), 837–856. https://doi.org/10.1139/v71-142.
(30) Kuo, M.; Kamelamela, N.; Shultz, M. J. Rotational Structure of Water in a Hydrophobic Environment: Carbon Tetrachloride. *J. Phys. Chem. A* **2008**, *112* (6), 1214–1218. https://doi.org/10.1021/jp7097284.
(31) Liang, C.; Kwak, K.; Cho, M. Revealing the Solvation Structure and Dynamics of Carbonate Electrolytes in Lithium-Ion Batteries by Two-Dimensional Infrared Spectrum Modeling. *J. Phys. Chem. Lett.* **2017**, *8* (23), 5779–5784. https://doi.org/10.1021/acs.jpclett.7b02623.
(32) Hayes, R.; Warr, G. G.; Atkin, R. Structure and Nanostructure in Ionic Liquids. *Chem. Rev.* **2015**, *115* (13), 6357–6426. https://doi.org/10.1021/cr500411q.
(33) Giorgini, M. G.; Futamatagawa, K.; Torii, H.; Musso, M.; Cerini, S. Solvation Structure around the Li+ Ion in Mixed Cyclic/Linear Carbonate Solutions Unveiled by the Raman Noncoincidence Effect. *J. Phys. Chem. Lett.* **2015**, *6* (16), 3296–3302. https://doi.org/10.1021/acs.jpclett.5b01524.
(34) Naji, A.; Ghanbaja, J.; Willmann, P.; Billaud, D. New Halogenated Additives to Propylene Carbonate-Based Electrolytes for Lithium-Ion Batteries. *Electrochimica Acta* **2000**, *45* (12), 1893–1899. https://doi.org/10.1016/S0013-4686(99)00410-7.
(35) Tasaki, K.; Goldberg, A.; Winter, M. On the Difference in Cycling Behaviors of Lithium-Ion Battery Cell between the Ethylene Carbonate- and Propylene Carbonate-Based Electrolytes. *Electrochimica Acta* **2011**, *56* (28), 10424–10435. https://doi.org/10.1016/j.electacta.2011.05.112.
(36) Aurbach, D.; Zaban, A. Impedance Spectroscopy of Lithium Electrodes: Part 1. General Behavior in Propylene Carbonate Solutions and the Correlation to Surface Chemistry and Cycling Efficiency. *J. Electroanal. Chem.* **1993**, *348* (1), 155–179. https://doi.org/10.1016/0022-0728(93)80129-6.
(37) Battisti, D.; Nazri, G. A.; Klassen, B.; Aroca, R. Vibrational Studies of Lithium Perchlorate in Propylene Carbonate Solutions. *J. Phys. Chem.* **1993**, *97* (22), 5826–5830. https://doi.org/10.1021/j100124a007.

(38) Xuan, X.; Wang, J.; Tang, J.; Qu, G.; Lu, J. A Vibrational Spectroscopic Study of Ion Solvation in Lithium Perchlorate/Propylene Carbonate Electrolyte. *Phys. Chem. Liq.* **2001**, *39* (3), 327–342. https://doi.org/10.1080/00319100108031666.
(39) Brennan, M. D.; Breedon, M.; Best, A. S.; Morishita, T.; Spencer, M. J. S. Surface Reactions of Ethylene Carbonate and Propylene Carbonate on the Li(001) Surface. *Electrochimica Acta* **2017**, *243*, 320–330. https://doi.org/10.1016/j.electacta.2017.04.163.
(40) Fulfer, K. D.; Kuroda, D. G. Solvation Structure and Dynamics of the Lithium Ion in Organic Carbonate-Based Electrolytes: A Time-Dependent Infrared Spectroscopy Study. *J. Phys. Chem. C* **2016**, *120* (42), 24011–24022. https://doi.org/10.1021/acs.jpcc.6b08607.
(41) Fulfer, K. D.; Galle Kankanamge, S. R.; Chen, X.; Woodard, K. T.; Kuroda, D. G. Elucidating the Mechanism behind the Infrared Spectral Features and Dynamics Observed in the Carbonyl Stretch Region of Organic Carbonates Interacting with Lithium Ions. *J. Chem. Phys.* **2021**, *154* (23), 234504. https://doi.org/10.1063/5.0049742.
(42) Stich, M.; Göttlinger, M.; Kurniawan, M.; Schmidt, U.; Bund, A. Hydrolysis of LiPF6 in Carbonate-Based Electrolytes for Lithium-Ion Batteries and in Aqueous Media. *J. Phys. Chem. C* **2018**, *122* (16), 8836–8842. https://doi.org/10.1021/acs.jpcc.8b02080.
(43) Li, W.; Lucht, B. L. Inhibition of the Detrimental Effects of Water Impurities in Lithium-Ion Batteries. *Electrochem. Solid-State Lett.* **2007**, *10* (4), A115. https://doi.org/10.1149/1.2458913.
(44) Hwang, S.; Kim, D.-H.; Shin, J. H.; Jang, J. E.; Ahn, K. H.; Lee, C.; Lee, H. Ionic Conduction and Solution Structure in LiPF6 and LiBF4 Propylene Carbonate Electrolytes. *J. Phys. Chem. C* **2018**, *122* (34), 19438–19446. https://doi.org/10.1021/acs.jpcc.8b06035.
(45) Wang, J.; Gu, W.; Chen, X.; Yang, M.; Chen, J.; Zhao, M.; Liu, Q.-S. Electrical Conductivity and Refractive Index of Binary Ionic Liquid Mixtures with Diethyl Carbonate, Dimethyl Carbonate and Propylene Carbonate. *J. Mol. Liq.* **2023**, *378*, 121598. https://doi.org/10.1016/j.molliq.2023.121598.
(46) Stoppa, A.; Hunger, J.; Buchner, R. Conductivities of Binary Mixtures of Ionic Liquids with Polar Solvents. *J. Chem. Eng. Data* **2009**, *54* (2), 472–479. https://doi.org/10.1021/je800468h.
(47) Matsumoto, R.; Thompson, M. W.; Cummings, P. T. Ion Pairing Controls Physical Properties of Ionic Liquid-Solvent Mixtures. *J. Phys. Chem. B* **2019**, *123* (46), 9944–9955. https://doi.org/10.1021/acs.jpcb.9b08509.
(48) Canongia Lopes, J. N.; Costa Gomes, M. F.; Husson, P.; Pádua, A. A. H.; Rebelo, L. P. N.; Sarraute, S.; Tariq, M. Polarity, Viscosity, and Ionic Conductivity of Liquid Mixtures Containing [C4C1im][Ntf2] and a Molecular Component. *J. Phys. Chem. B* **2011**, *115* (19), 6088–6099. https://doi.org/10.1021/jp2012254.
(49) Muhuri, P. K.; Ghosh, S. K.; Hazra, D. K. Solubilities of Some Alkali-Metal Salts, Tetraphenylarsonium Chloride, and Tetraphenylphosphonium Bromide in Propylene Carbonate at 25.Degree.C Using the Ion-Selective Electrode Technique. *J. Chem. Eng. Data* **1993**, *38* (2), 242–244. https://doi.org/10.1021/je00010a014.
(50) Carey, D. M.; Korenowski, G. M. Measurement of the Raman Spectrum of Liquid Water. *J. Chem. Phys.* **1998**, *108* (7), 2669–2675. https://doi.org/10.1063/1.475659.
(51) Wang, Z.; Pakoulev, A.; Pang, Y.; Dlott, D. D. Vibrational Substructure in the OH Stretching Band of Water. *Chem. Phys. Lett.* **2003**, *378* (3), 281–288. https://doi.org/10.1016/S0009-2614(03)01267-3.
(52) Sun, Q. The Raman OH Stretching Bands of Liquid Water. *Vib. Spectrosc.* **2009**, *51* (2), 213–217. https://doi.org/10.1016/j.vibspec.2009.05.002.

(53) Liu, D.; Ma, G.; Levering, L. M.; Allen, H. C. Vibrational Spectroscopy of Aqueous Sodium Halide Solutions and Air−Liquid Interfaces: Observation of Increased Interfacial Depth. *J. Phys. Chem. B* **2004**, *108* (7), 2252–2260. https://doi.org/10.1021/jp036169r.
(54) Kecki, Z.; Sokołowska, A. Crossing of Anisotropic and Isotropic Raman Components in the Intermolecular Resonance Coupling of Vibrations. IV—Methanol Solutions in Acetone. *J. Raman Spectrosc.* **1996**, *27* (5), 429–432. https://doi.org/10.1002/(SICI)1097-4555(199605)27:5<429::AID-JRS981>3.0.CO;2-O.
(55) Nicodemus, R. A.; Ramasesha, K.; Roberts, S. T.; Tokmakoff, A. Hydrogen Bond Rearrangements in Water Probed with Temperature-Dependent 2D IR. *J. Phys. Chem. Lett.* **2010**, *1* (7), 1068–1072. https://doi.org/10.1021/jz100138z.
(56) Burikov, S.; Dolenko, T.; Patsaeva, S.; Starokurov, Y.; Yuzhakov, V. Raman and IR Spectroscopy Research on Hydrogen Bonding in Water-Ethanol Systems. *Mol. Phys.* **2010**, *108* (18), 2427–2436. https://doi.org/10.1080/00268976.2010.516277.
(57) Sun, Q. Local Statistical Interpretation for Water Structure. *Chem. Phys. Lett.* **2013**, *568–569*, 90–94. https://doi.org/10.1016/j.cplett.2013.03.065.
(58) Sun, Q.; Qin, C. Raman OH Stretching Band of Water as an Internal Standard to Determine Carbonate Concentrations. *Chem. Geol.* **2011**, *283* (3), 274–278. https://doi.org/10.1016/j.chemgeo.2011.01.025.
(59) Hendrikse, R. L.; Bayly, A. E.; Jimack, P. K.; Lai, X. Using Raman Spectroscopy and Molecular Dynamics to Study Conformation Changes of Sodium Lauryl Ether Sulfate Molecules. *J. Phys. Chem. B* **2023**, *127* (20), 4676–4686. https://doi.org/10.1021/acs.jpcb.3c02022.
(60) Auer, B.; Kumar, R.; Schmidt, J. R.; Skinner, J. L. Hydrogen Bonding and Raman, IR, and 2D-IR Spectroscopy of Dilute HOD in Liquid D2O. *Proc. Natl. Acad. Sci.* **2007**, *104* (36), 14215–14220. https://doi.org/10.1073/pnas.0701482104.
(61) Corcelli, S. A.; Skinner, J. L. Infrared and Raman Line Shapes of Dilute HOD in Liquid H2O and D2O from 10 to 90 C. *J. Phys. Chem. A* **2005**, *109* (28), 6154–6165.
(62) Devlin, J. P.; Sadlej, J.; Buch, V. Infrared Spectra of Large H2O Clusters: New Understanding of the Elusive Bending Mode of Ice. *J. Phys. Chem. A* **2001**, *105* (6), 974–983. https://doi.org/10.1021/jp003455j.
(63) Perakis, F.; De Marco, L.; Shalit, A.; Tang, F.; Kann, Z. R.; Kühne, T. D.; Torre, R.; Bonn, M.; Nagata, Y. Vibrational Spectroscopy and Dynamics of Water. *Chem. Rev.* **2016**, *116* (13), 7590–7607. https://doi.org/10.1021/acs.chemrev.5b00640.
(64) Paesani, F.; Xantheas, S. S.; Voth, G. A. Infrared Spectroscopy and Hydrogen-Bond Dynamics of Liquid Water from Centroid Molecular Dynamics with an Ab Initio-Based Force Field. *J. Phys. Chem. B* **2009**, *113* (39), 13118–13130. https://doi.org/10.1021/jp907648y.
(65) *Propylene carbonate anhydrous, 99.7 108-32-7*. https://www.sigmaaldrich.com/US/en/product/sial/310328?gclid=Cj0KCQiAyracBhDoARIsACGFcS7weCHAT5_OlIWtLy6JvNcz06-j4DeGkq5UR4t4DxbnhJnzKzSJ-YMaAmauEALw_wcB&gclsrc=aw.ds (accessed 2022-12-05).
(66) Baumler, S. M.; V, W. H. H.; Allen, H. C. Hydration of Ferric Chloride and Nitrate in Aqueous Solutions: Water-Mediated Ion Pairing Revealed by Raman Spectroscopy. *Phys. Chem. Chem. Phys.* **2019**, *21* (35), 19172–19180. https://doi.org/10.1039/C9CP01392J.
(67) Berendsen, H. J. C.; Grigera, J. R.; Straatsma, T. P. The Missing Term in Effective Pair Potentials. *J. Phys. Chem.* **1987**, *91* (24), 6269–6271. https://doi.org/10.1021/j100308a038.
(68) Schuler, L. D.; Daura, X.; van Gunsteren, W. F. An Improved GROMOS96 Force Field for Aliphatic Hydrocarbons in the Condensed Phase. *J. Comput. Chem.* **2001**, *22* (11), 1205–1218. https://doi.org/10.1002/jcc.1078.

(69) Parrinello, M.; Rahman, A. Polymorphic Transitions in Single Crystals: A New Molecular Dynamics Method. *J. Appl. Phys.* **1981**, *52* (12), 7182–7190. https://doi.org/10.1063/1.328693.
(70) Martyna, G. J.; Tobias, D. J.; Klein, M. L. Constant Pressure Molecular Dynamics Algorithms. *J. Chem. Phys.* **1994**, *101* (5), 4177–4189. https://doi.org/10.1063/1.467468.
(71) Andersen, H. C. Rattle: A "Velocity" Version of the Shake Algorithm for Molecular Dynamics Calculations. *J. Comput. Phys.* **1983**, *52* (1), 24–34. https://doi.org/10.1016/0021-9991(83)90014-1.
(72) Eaves, J. D.; Loparo, J. J.; Fecko, C. J.; Roberts, S. T.; Tokmakoff, A.; Geissler, P. L. Hydrogen Bonds in Liquid Water Are Broken Only Fleetingly. *Proc. Natl. Acad. Sci.* **2005**, *102* (37), 13019–13022. https://doi.org/10.1073/pnas.0505125102.
(73) Geissler, P. L. Water Interfaces, Solvation, and Spectroscopy. *Annu. Rev. Phys. Chem.* **2013**, *64* (1), 317–337. https://doi.org/10.1146/annurev-physchem-040412-110153.
(74) Smith, J. D.; Saykally, R. J.; Geissler, P. L. The Effects of Dissolved Halide Anions on Hydrogen Bonding in Liquid Water. *J. Am. Chem. Soc.* **2007**, *129* (45), 13847–13856. https://doi.org/10.1021/ja071933z.
(75) Hess, B.; van der Vegt, N. F. A. Hydration Thermodynamic Properties of Amino Acid Analogues: A Systematic Comparison of Biomolecular Force Fields and Water Models. *J. Phys. Chem. B* **2006**, *110* (35), 17616–17626. https://doi.org/10.1021/jp0641029.
(76) Tomlinson-Phillips, J.; Davis, J.; Ben-Amotz, D.; Spångberg, D.; Pejov, L.; Hermansson, K. Structure and Dynamics of Water Dangling OH Bonds in Hydrophobic Hydration Shells. Comparison of Simulation and Experiment. *J. Phys. Chem. A* **2011**, *115* (23), 6177–6183. https://doi.org/10.1021/jp111346s.
(77) Stirnemann, G.; Rossky, P. J.; Hynes, J. T.; Laage, D. Water Reorientation, Hydrogen-Bond Dynamics and 2D-IR Spectroscopy next to an Extended Hydrophobic Surface. *Faraday Discuss.* **2010**, *146* (0), 263–281. https://doi.org/10.1039/B925673C.
(78) Perera, P. N.; Fega, K. R.; Lawrence, C.; Sundstrom, E. J.; Tomlinson-Phillips, J.; Ben-Amotz, D. Observation of Water Dangling OH Bonds around Dissolved Nonpolar Groups. *Proc. Natl. Acad. Sci.* **2009**, *106* (30), 12230–12234. https://doi.org/10.1073/pnas.0903675106.
(79) Ma, G.; Chen, X.; Allen, H. C. Dangling OD Confined in a Langmuir Monolayer. *J. Am. Chem. Soc.* **2007**, *129* (45), 14053–14057. https://doi.org/10.1021/ja075806e.
(80) Scatena, L. F.; Brown, M. G.; Richmond, G. L. Water at Hydrophobic Surfaces: Weak Hydrogen Bonding and Strong Orientation Effects. *Science* **2001**, *292* (5518), 908–912.
(81) Medders, G. R.; Paesani, F. Dissecting the Molecular Structure of the Air/Water Interface from Quantum Simulations of the Sum-Frequency Generation Spectrum. *J. Am. Chem. Soc.* **2016**, *138* (11), 3912–3919.
(82) Sun, S.; Tang, F.; Imoto, S.; Moberg, D. R.; Ohto, T.; Paesani, F.; Bonn, M.; Backus, E. H.; Nagata, Y. Orientational Distribution of Free OH Groups of Interfacial Water Is Exponential. *Phys. Rev. Lett.* **2018**, *121* (24), 246101.
(83) Zischang, J.; Suhm, M. A. The OH Stretching Spectrum of Warm Water Clusters. *J. Chem. Phys.* **2014**, *140* (6), 064312. https://doi.org/10.1063/1.4865130.
(84) Buck, U.; Pradzynski, C. C.; Zeuch, T.; Dieterich, J. M.; Hartke, B. A Size Resolved Investigation of Large Water Clusters. *Phys. Chem. Chem. Phys.* **2014**, *16* (15), 6859–6871. https://doi.org/10.1039/C3CP55185G.
(85) Senanayake, H. S.; Greathouse, J. A.; Ilgen, A. G.; Thompson, W. H. Simulations of the IR and Raman Spectra of Water Confined in Amorphous Silica Slit Pores. *J. Chem. Phys.* **2021**, *154* (10), 104503. https://doi.org/10.1063/5.0040739.

(86) Morawietz, T.; Marsalek, O.; Pattenaude, S. R.; Streacker, L. M.; Ben-Amotz, D.; Markland, T. E. The Interplay of Structure and Dynamics in the Raman Spectrum of Liquid Water over the Full Frequency and Temperature Range. *J. Phys. Chem. Lett.* **2018**, *9* (4), 851–857. https://doi.org/10.1021/acs.jpclett.8b00133.
(87) Luzar, A.; Chandler, D. Effect of Environment on Hydrogen Bond Dynamics in Liquid Water. *Phys. Rev. Lett.* **1996**, *76* (6), 928–931. https://doi.org/10.1103/PhysRevLett.76.928.
(88) Fecko, C. J.; Eaves, J. D.; Loparo, J. J.; Tokmakoff, A.; Geissler, P. L. Ultrafast Hydrogen-Bond Dynamics in the Infrared Spectroscopy of Water. *Science* **2003**, *301* (5640), 1698–1702. https://doi.org/10.1126/science.1087251.
(89) Asbury, J. B.; Steinel, T.; Stromberg, C.; Corcelli, S. A.; Lawrence, C. P.; Skinner, J. L.; Fayer, M. D. Water Dynamics: Vibrational Echo Correlation Spectroscopy and Comparison to Molecular Dynamics Simulations. *J. Phys. Chem. A* **2004**, *108* (7), 1107–1119. https://doi.org/10.1021/jp036266k.
(90) Corcelli, S. A.; Lawrence, C. P.; Skinner, J. L. Combined Electronic Structure/Molecular Dynamics Approach for Ultrafast Infrared Spectroscopy of Dilute HOD in Liquid H2O and D2O. *J. Chem. Phys.* **2004**, *120* (17), 8107–8117. https://doi.org/10.1063/1.1683072.
(91) Janz, G. J.; Ambrose, J.; Coutts, J. W.; Downey, J. R. Raman Spectrum of Propylene Carbonate. *Spectrochim. Acta Part Mol. Spectrosc.* **1979**, *35* (2), 175–179. https://doi.org/10.1016/0584-8539(79)80181-6.
(92) Carter-Fenk, K. A.; Dommer, A. C.; Fiamingo, M. E.; Kim, J.; Amaro, R. E.; Allen, H. C. Calcium Bridging Drives Polysaccharide Co-Adsorption to a Proxy Sea Surface Microlayer. *Phys. Chem. Chem. Phys.* **2021**, *23* (30), 16401–16416. https://doi.org/10.1039/D1CP01407B.
(93) Dreier, L. B.; Bonn, M.; Backus, E. H. G. Hydration and Orientation of Carbonyl Groups in Oppositely Charged Lipid Monolayers on Water. *J. Phys. Chem. B* **2019**, *123* (5), 1085–1089. https://doi.org/10.1021/acs.jpcb.8b12297.
(94) Edington, S. C.; Flanagan, J. C.; Baiz, C. R. An Empirical IR Frequency Map for Ester C═O Stretching Vibrations. *J. Phys. Chem. A* **2016**, *120* (22), 3888–3896. https://doi.org/10.1021/acs.jpca.6b02887.
(95) Giorgini, M. G.; Torii, H.; Musso, M.; Venditti, G. Influence of Ions on the Structural Organization of Dipolar Liquids Probed by the Noncoincidence Effect: Experimental and Quantum Chemical Results. *J. Phys. Chem. B* **2008**, *112* (25), 7506–7514. https://doi.org/10.1021/jp800252n.
(96) Vazquez de Vasquez, M. G.; Wellen Rudd, B. A.; Baer, M. D.; Beasley, E. E.; Allen, H. C. Role of Hydration in Magnesium versus Calcium Ion Pairing with Carboxylate: Solution and the Aqueous Interface. *J. Phys. Chem. B* **2021**, *125* (40), 11308–11319. https://doi.org/10.1021/acs.jpcb.1c06108.
(97) Brodin, A.; Jacobsson, P. Dipolar Interaction and Molecular Ordering in Liquid Propylene Carbonate: Anomalous Dielectric Susceptibility and Raman Non-Coincidence Effect. *J. Mol. Liq.* **2011**, *164* (1), 17–21. https://doi.org/10.1016/j.molliq.2011.08.001.
(98) Ladanyi, B. M.; Geiger, L. C.; Zerda, T. W.; Song, X.; Jonas, J. Experimental and Molecular Dynamics Study of the Pressure Dependence of Raman Spectra of Oxygen. *J. Chem. Phys.* **1988**, *89* (2), 660–672. https://doi.org/10.1063/1.455241.
(99) Giorgini, M. G.; Torii, H.; Musso, M. The Influence of Alkaline Earth Ions on the Structural Organization of Acetone Probed by the Noncoincidence Effect of the ν(CO) Band: Experimental and Quantum Chemical Results. *Phys. Chem. Chem. Phys.* **2009**, *12* (1), 183–192. https://doi.org/10.1039/B912164A.